

DMD # 87759

Specificity of the redox complex between cytochrome P450 24A1 and adrenodoxin relies on carbon-25 hydroxylation of vitamin-D substrate

Amit Kumar¹, D. Fernando Estrada¹

1. Department of Biochemistry, Jacobs School of Medicine and Biomedical Science, University at Buffalo, Buffalo NY 14203

DMD # 87759

Running title: vitamin-D modulates the CYP24A1-Adx protein interaction

Correspondence to: D. Fernando Estrada, Department of Biochemistry, Jacobs School of Medicine and Biomedical Science, University at Buffalo, Buffalo NY 14203;
dfestrad@buffalo.edu; phone (716) 829-2767; fax (716) 829-2725.

Pages of text	24
Tables	0
Figures	8
References	39
Words in Abstract	255
Words in Introduction	467
Words in Discussion	1,058

Nonstandard abbreviations:

Adx	rat adrenodoxin
b_5	cytochrome b_5
CPR	cytochrome P450 oxidoreductase
CYP	cytochrome P450
CYP24A1	cytochrome P450 24A1
HSQC	heteronuclear single quantum coherence
[2Fe-2S]	iron sulfur cluster

DMD # 87759

Abstract

Metabolic deactivation of 1,25(OH)₂D₃ is initiated by modification of the vitamin-D side chain, as carried out by the mitochondrial cytochrome P450 24A1 (CYP24A1). In addition to its role in vitamin-D metabolism, CYP24A1 is involved in catabolism of vitamin-D analogs, thereby reducing their efficacy. CYP24A1 function relies on electron transfer from the soluble ferredoxin protein adrenodoxin (Adx). Recent structural evidence suggests that regioselectivity of the CYP24A1 reaction may correlate with distinct modes of Adx recognition. Here we use nuclear magnetic resonance (NMR) spectroscopy to monitor the structure of ¹⁵N labeled full-length Adx from rat while forming the complex with rat CYP24A1 in the ligand-free state or bound to either 1,25(OH)₂D₃ or the vitamin-D supplement 1α(OH)D₃. While both vitamin-D ligands were found to induce a reduction in overall NMR peak broadening, thereby suggesting ligand-induced disruption of the complex, a cross-linking analysis suggests that ligand does not have a significant effect on the relative association affinities of the redox complexes. However, a key finding is that, while the presence of primary CYP24A1 substrate was found to induce NMR peak broadening focused on the putative recognition site α-helix 3 of Adx, the interaction in the presence of 1α(OH)D₃, which is lacking the carbon-25 hydroxyl, results in disruption of the NMR peak broadening pattern, thus indicating a ligand-induced non-specific protein interaction. These findings provide a structural basis for the poor substrate turnover of side chain modified vitamin-D analogs, while also confirming that specificity of the CYP24A1-ligand interaction influences specificity of CYP24A1-Adx recognition.

DMD # 87759

Significance Statement:

Mitochondrial cytochrome P450 enzymes, such as CYP24A1 responsible for catabolizing vitamin-D and its analogs, rely on a protein-protein interaction with a ferredoxin in order to receive delivery of the electrons required for catalysis. In this study, we demonstrate that this protein interaction is influenced by the enzyme-ligand interaction that precedes it. Specifically, vitamin-D missing carbon-25 hydroxylation binds the enzyme active site with high affinity, but results in a loss of CYP-ferredoxin binding specificity.

DMD # 87759

Introduction

The bioactive form of vitamin-D, 1,25(OH)₂D₃, is responsible for the maintenance of calcium and phosphate homeostasis, with insufficiency of the hormone causing vitamin-D dependent rickets and osteomalacia, among other diseases (Holick, 2007; Ryan et al., 2013). The metabolic stability of 1,25(OH)₂D₃ relies on the activity of the multifunctional mitochondrial enzyme CYP24A1, which initiates deactivation of the hormone by mediating modification of the 1,25(OH)₂D₃ side chain to produce either carbon-23 (C23) or carbon-24 (C24) hydroxylation products (Siu-Caldera et al., 1995; Beckman et al., 1996). While the human isoform is both a C23 and C24 hydroxylase, in other species regioselectivity is divided between either C23 or C24 pathways (Hamamoto et al., 2006; Prosser et al., 2007). Subsequent activity by CYP24A1 includes catalysis of all ensuing steps for each pathway to produce either calcitroic acid (C24) or the vitamin-D receptor antagonist 1,25(OH)₂D₃-26,23-lactone (C23). Due to its central role in vitamin-D metabolism, the function of CYP24A1 is a primary concern in the development of vitamin-D analogs designed to therapeutically treat vitamin-D deficiency. The ideal analog must maintain signaling activity via its interaction with the vitamin-D receptor, yet must also be catalytically resistant (therefore metabolically stable) with regard to modification by CYP24A1.

Like most cytochrome P450 enzymes (CYPs), CYP24A1 catalysis requires sequential transfer of two external electrons in order to reduce the heme iron and produce the reactive Fe(IV)oxo intermediate. In mitochondria, these reduction steps necessitate an interaction with the water-soluble [2Fe-2S] protein adrenodoxin (Adx) (Ewen et al., 2011). We recently reported an analysis of the interaction between CYP24A1 and Adx by NMR spectroscopy, in which clotrimazole-bound CYP24A1 isoforms from species with different regioselectivity for 1,25(OH)₂D₃ were found to rely on distinct secondary contacts for the protein-protein complex (Estrada, 2018). This finding suggested a correlation between site-specific regioselective hydroxylation of the substrate with recognition of the redox partner; a feature that we

DMD # 87759

hypothesize would require structural communication between the active site and the opposite (proximal) surface of the enzyme.

In this study, we seek to confirm the existence of substrate induced two-way communication between the active site and the Adx recognition surface of CYP24A1. We've monitored the protein interaction using 2D NMR and by incorporating ligand-free CYP24A1 or CYP24A1 bound to either 1,25(OH)₂D3 or the vitamin-D supplement 1α(OH)D3. 1α(OH)D3 is of particular interest as a functional probe because it retains high affinity for CYP24A1, yet is an extremely poor substrate when compared to 1,25(OH)₂D3 (Kaufmann et al., 2011). Comparative mapping of the peak-broadening pattern from the ¹⁵N-Adx signal demonstrates that 1,25(OH)₂D3 enhances the specificity of the interaction, as reflected by focused mapping of the interaction on α-helix 3 of Adx, but that the absence of a carbon-25 hydroxyl from 1α(OH)D3 makes the interaction structurally and functionally non-specific. These findings represent direct biophysical evidence of substrate-driven allostery in a critical vitamin-D metabolizing CYP.

DMD # 87759

Material and Methods

Protein expression and purification

The gene encoding full-length rat Adx (GenBank accession number **NP_05882.1**) was modified to contain a C-terminal poly-histidine tag and was custom synthesized (Genscript) and cloned into a pET-15b expression vector (Novagen). Overexpression and purification of ^{15}N - Adx was carried out as described previously (Estrada, 2018). Backbone assignment of Adx required ^{15}N and ^{13}C labeling, which was carried out by supplementing minimal growth media with 4 grams per liter of ^{13}C glucose and 1 gram per liter of ^{15}N ammonium chloride (Cambridge Isotope). Purity was determined by a A_{415}/A_{280} ratio greater than 0.8. Sample concentration was calculated using an extinction coefficient for the iron cofactor of $11 \text{ mM}^{-1} \text{ cm}^{-1}$. Single-residue mutations of rat Adx were also generated by Genscript and were purified identically to wild-type protein.

Generation of recombinant rat CYP24A1 (GenBank accession number **NP_963966.1**) was carried out similar to our previous protocol (Estrada, 2018) with the following modifications. Once CYP24A1 was bound to a saturated Adx-affinity Ni NTA column, the column was washed using 5 column volumes of equilibration buffer (10 mM potassium phosphate, 20% glycerol, 0.1 % 3-[(3-cholamidopropyl)dimethylammonio]-1-propanesulfonate (CHAPS), 2 mM β -mercaptoethanol, pH 7.4) followed by 5 column volumes at 30% elution buffer (500 mM potassium phosphate, 300 mM NaCl, 20% glycerol, 0.1 % CHAPS, 2 mM β -mercaptoethanol, pH 7.4). The protein was then recovered using 100% elution buffer, in which the high salt concentration effectively disrupts the CYP24A1-Adx interaction of the Adx-affinity column. Subsequent purification by gel filtration was carried out in the same affinity elution buffer and produced a protein purity ratio (A_{417}/A_{280}) greater than 1.0 (Supplemental Figure 7-A).

DMD # 87759

NMR assignment and homology modeling of Adx

Data acquisitions of 2D and 3D experiments were carried out at 25 °C on a Varian Inova 600-MHz spectrometer equipped with a cryogenic probe. A sample of ¹⁵N and ¹³C labeled Adx was exchanged into NMR buffer consisting of 50 mM potassium phosphate (pH 6.8) and 50 mM NaCl, 10% D₂O, and was brought to 2.6 mM protein concentration. Data sets used to assign the protein backbone consisted of HSQC, HNCA, HNCACB and HNCOCA experiments (Bax and Ikura, 1991; Grzesiek et al., 1992; Constantine et al., 1993; Grzesiek et al., 1993). The data were processed using nmrPipe (Delaglio et al., 1995) and the processed spectra were analyzed on NMRViewJ (Johnson, 2004). The ¹⁵N and ¹³C chemical shift values determined during assignment of the protein have been submitted to the Biological Magnetic Resonance Data Bank (BMRB) (ID number 27673). Secondary chemical shift values (C α) were used to predict secondary structural elements (Wishart and Sykes, 1994). Due to the high degree of similarity between chemical shift predictions of the backbone secondary structure with that of the reported crystal structure of bovine Adx (Pikuleva et al., 2000), the bovine structure (PDB ID ICJE) was used as a template for homology modeling of rat Adx using the I-TASSER and SWISS-MODEL servers (Yang et al., 2015; Waterhouse et al., 2018). The modeled Adx structure was then validated using PROCHECK (Laskowski et al., 1996).

Spectral ligand binding assays

Binding of calcitriol or alfacalcidol (both from ApexBio) to CYP24A1 was carried out as described previously with minor modifications (Estrada, 2018). Briefly, ligand binding was measured by monitoring perturbation of the Soret peak at incremental concentrations of ligand. Binding assays were carried out in triplicate with CYP24A1 in gel filtration buffer, concentrated to X mg/ml, then diluted to 1 μ M in 100 mM potassium phosphate, pH 7.4. Ligand titrations (between 0-8 μ M) were added from a DMSO stock with total DMSO contributing to 1.6 % of total sample volume. At each concentration, the enzyme and ligand were incubated for 12 minutes at

DMD # 87759

25 °C prior to recording of absorption spectra on a Shimadzu UV-2700 spectrophotometer. Baseline-subtracted difference spectra showing a maximum and a minimum at 385nm and 418nm were used to generate total spectral response, which was then plotted against ligand concentration to generate total binding data. Binding constants were then calculated upon fitting data using Prism 7.02 (GraphPad software) to the saturation binding equation with ligand depletion shown below, in which $a = -1.0$, $b = Kd + X + B_{max}$, and $c = -1 \cdot X \cdot B_{max}$, and $X = total\ ligand\ added$.

$$Total\ binding = -b + \sqrt{(b^2 - 4 \cdot a \cdot c)} / (2 \cdot a)$$

NMR titration of ¹⁵N-Adx with CYP24A1

All ¹⁵N-HSQC spectra were acquired using a final concentration of 100 μM of ¹⁵N-Adx. As described earlier (Estrada, 2018), a specific sequence of steps for buffer exchange was carefully followed in order to ensure that extraneous unbound detergent is removed from CYP24A1 samples prior to combining with 50 nmoles of ¹⁵N-Adx. Briefly, CYP24A1 was first exchanged into a high salt, detergent free buffer by a 10-fold volume exchange through a 50 kDa filter (Amicon), then combined with ¹⁵N-Adx (100 μM) and exchanged into low salt NMR sample buffer by a 10-fold volume exchange through a 10 kDa filter. NMR spectra of mutant ¹⁵N-Adx were acquired using the same protocol. As observed previously, the stoichiometric excess of ¹⁵N-Adx to CYP24A1 (1:0.2 or 1:0.4) conferred stability on the CYP. Following each data acquisition, each sample was recovered and the CYP quantified spectrophotometrically, with no significant loss of CYP24A1 detected. Samples containing either 1,25(OH)₂D3 or 1α(OH)D3 were prepared using the same procedure, but with an excess concentration of ligand (50 μM ligand combined with 20 or 40 μM CYP24A1) introduced during exchange into NMR buffer. The absorption spectra of ligand-bound CYP24A1 samples were monitored upon completion of data collection (Supplemental Figure 1) in order to ensure that ligand remained bound during NMR data acquisition.

DMD # 87759

Each spectrum was acquired using 96 scans and 128 increments, with a total acquisition time of 4.5 hours per experiment. The peak intensities corresponding to each assigned amide were quantified from the processed spectra and the values expressed as a ratio of remaining intensity using the following formula:

$$I_{\text{remaining}} = I_{\text{CYP added}} / I_{\text{free}}$$

From these values, differential peak broadening was identified using either 0.75 or 1 full standard deviation from the mean of the remaining intensities. For representations of net peak broadening across the entire Adx structure, individual residue peak ratios were treated as separate data points and graphed in box plots. Box plots were generated using Interactive Dotplot (<http://statistika.mfub.bg.ac.rs/interactive-dotplot/>) (Weissgerber et al., 2017).

Chemical cross-linking

Purified rat CYP24A1 was incubated with rat Adx under low-salt conditions (10 mM potassium phosphate buffer, pH 7.4) and in the presence of the zero length cross-linker 1-Ethyl-3-(3-dimethylaminopropyl)carbodiimide (EDC) (Thermo Scientific). In order to compare cross-linking data with complex formation by NMR, the protein ratios were kept consistent with those used for NMR binding data. Specifically, each reaction was run in triplicate using 8 μM and 16 μM of ligand bound and unliganded CYP corresponding to 1:0.2 and 1: 0.4 ratios respectively, combined with 40 μM of Adx in a 20 μl reaction volume. After a 2-hour incubation period at 25 $^{\circ}\text{C}$, the reaction was terminated by addition of an equal volume of Laemmli loading dye. The samples were then resolved by gel electrophoresis and stained with Coomassie Blue. The protein bands were quantified by Image Lab™ 6.0 (Bio-Rad). Cross-linking efficiency was

DMD # 87759

calculated as a ratio of band volume of the cross-linked product divided by total band volume of the complex, CYP24A1, and Adx combined. Saturation curves were obtained by titrating CYP24A1 between 0 and 20 μM against a fixed concentration of 40 μM Adx and quantified as a ratio of the volume of the complex band to that of a loading control of CYP24A1 alone. The curves were fitted using a one-site specific binding equation in Prism 5.0 (GraphPad).

CYP24A1 functional assays

Reconstituted CYP24A1 assays were carried out in 100 μl volumes and contained either equal concentrations (1.5 μM each) of rat CYP24A1, rat Adx, and bovine adrenodoxin reductase, or reduced CYP24A1 in order to match the protein ratios captured by NMR. 1,25(OH)₂D₃ and 1 α (OH)D₃ were kept constant at 5 μM . The reaction mixtures were first pre-incubated for 5 minutes at 37 °C, then initiated by addition of NADPH to a final concentration of 1 mM. After a further 5 minute incubation at 37 °C, the reactions were terminated by addition of 2 volumes of methanol. Internal standards were then added to a final concentration of 2 μM . 25(OH)D₃ was used as an internal standard for reactions containing 1,25(OH)₂D₃ as substrate while 1,25(OH)₂D₃ was used as an internal standard for reactions containing 1 α (OH)D₃ as substrate. Samples were subjected to centrifugation at 34,000 *g* for 30 minutes and 150 μl of the supernatant was removed and diluted with additional methanol to a final volume of 200 μl . HPLC samples were resolved on an Agilent 1260 Infinity II liquid chromatography system with a Poroshell 120 EC-C18 column (4.6 x 250 mm) and using an isocratic mobile phase of 70% acetonitrile, 30% water. Elution peaks were detected by monitoring absorbance at 264 nm. All samples were run in quadruplicate and the remaining substrate for each was calculated as a percentage of substrate measured from a control sample in which CYP24A1 was withheld.

DMD # 87759

Accumulation of H₂O₂ was measured in quadruplicate using a colorimetric assay (Pierce Quantitative Peroxide Assay Kit, #23280), with a serial dilution of a 30% H₂O₂ solution used as a standard curve.

Results

NMR assignment and homology modeling of rat Adx

Recombinant human and bovine Adx have previously been characterized by NMR (Weiss et al., 2000; Kostic et al., 2002). However, in order to pair redox partners from the same species, we generated and characterized full-length (residues 1-128) ¹⁵N labeled Adx from rat, which shares approximately 85% sequence identity with bovine or human Adx. The ¹⁵N-HSQC spectrum of Adx is well dispersed with resolvable amide peaks and presents a similar 2D pattern as that of other species (Figure 1). However, due to ambiguities in transferring backbone chemical shift assignments from the BMRB database entries from related proteins, particularly in the crowded regions of the spectrum, the Adx NMR spectrum was assigned *ab initio* by analysis of three dimensional correlation experiments (HNCA, HNCACB, and HNCOCA). Overall, approximately 70% of the backbone amides of Adx were assigned, including residues for all three short helices of the core domain, with notable exceptions for residues located near the paramagnetic [2Fe-2S] coordination loop.

Secondary chemical shift values derived from NMR assignment of the α and β carbons of residue side chains (defined as $\Delta\delta = \delta_{\text{observed}} - \delta_{\text{random coil}}$) were used to predict the secondary structural elements of Adx (Wishart and Sykes, 1994). As expected, the secondary structure of rat Adx was found to align closely with that of bovine Adx (Supplemental Figure 2), suggesting a similar overall protein fold. Therefore, bovine Adx (PDB 1CJE, (Pikuleva et al., 2000)) was used as a template for structure prediction of rat Adx via I-TASSER (Yang et al., 2015). The modeled

DMD # 87759

structure (Figure 2A) conforms to the conserved Adx fold, with a core domain consisting of three short α -helices framing a solvent exposed [2Fe-2S] cluster.

Interaction of ^{15}N -Adx with ligand free CYP24A1

In order to establish the baseline redox partner interaction in the absence of ligand, we acquired 2D HSQC spectra of ^{15}N -Adx in the presence of increasing concentrations of ligand free CYP24A1. Similar to our previous binding data acquired with the clotrimazole-bound CYP24A1, unliganded CYP24A1 also induces considerable broadening of the NMR signal, with approximately 32% of the original signal intensity remaining upon addition of 0.2 molar equivalents of CYP24A1 (Figure 2B and Supplemental Figure 3). However, unlike the interaction with the inhibitor bound enzyme, unliganded CYP24A1 produces a modest amount of differential line broadening in which specific amide signals are differentially broadened. This broadening of signal is likely due to a combination of factors, including a protein interaction that undergoes intermediate chemical exchange, observed for protein complexes with dissociation constants between 1 and 10 μM , as well as an increase in the relative size of the observable ^{15}N -Adx when incorporated into the complex. However, differential broadening of NMR signal as a reporter of localized changes in the chemical environment has previously been demonstrated to correlate with functionally relevant CYP protein-protein binding interfaces (Estrada et al., 2013; Bart and Scott, 2017). Next, we mapped sites that are broadened greater than one standard deviation from the mean in response to addition of unliganded CYP24A1 (Figure 2, highlighted in red). The pattern presents as a contiguous surface on the solvent exposed side of α -helix 3 composed of Glu-73, Glu-74, Asp-76, and Asp-79. The interaction with ligand-free CYP24A1 was also observed to produce a secondary broadening effect on α -helix 1 (Figure 2A, highlighted in orange).

DMD # 87759

Effects of charge neutralizing mutations of ^{15}N -Adx on recognition of ligand free CYP24A1

We designed a series of charge neutralizing mutations in Adx as a way to assess contributions from particular anionic surface residues toward the redox interaction. Particular sites were selected for mutation based on their proximity to the iron center, and therefore their anticipated involvement in recognition of CYP24A1. Further consideration was given to the distribution of the mutations, with substitutions located on each of the adjacent helices. As such, substitutions were carried out at each of α -helices 1, 2 and 3 (D31N, E65Q, and D72N, respectively) as well as E47Q on the [2Fe-2S] coordinating loop. The structural integrity of each mutant was verified by overlaying of the ^{15}N -HSQC spectra with that of wild-type ^{15}N -Adx (Supplemental Figure 4). While some mutations expectedly induced minor or modest chemical shift perturbations in the spectrum of ^{15}N -Adx, none of the mutations disrupted the overall protein fold.

Next, we compared NMR spectra of free ^{15}N -Adx mutants with spectra of the mutants in the presence of 0.2 molar equivalents of CYP24A1 (Figure 3A, Table S1). We observed that substituting individual anionic side chains with uncharged polar side chains does not abolish the complex. Rather, we observe subtle re-distribution of peak broadening for the ^{15}N -Adx mutants. For example, the redox complex with mutation D72N on α -helix 3 results in a local re-distribution of peak broadening toward the C-terminal end of the helix, likely due to minor changes in complimentary charge pairing to compensate for the charge removal (α -helix 3 contains multiple conserved anionic surfaces). In contrast, the mutant E47Q, designed to remove the sole charge on the [2Fe-2S] coordinating loop, displays a peak broadening pattern very similar to that of wild-type.

Interestingly, mutations on α -helices 1 and 2 result in more pronounced changes in the broadening pattern. The mutant E65Q on α -helix 2 induces enhanced peak broadening at Val-

DMD # 87759

32 of α -helix 1. In contrast, the mutant D31N on α -helix 1 induces a *reduction* of peak broadening on Asp-76 of α -helix 3. A further analysis of net line broadening for each mutant ^{15}N -Adx spectra with CYP24A1 indicates that certain mutations of the Adx surface reduce overall complex formation (Figure 3B). These include the mutant at the expected recognition site, D72N, but also include secondary sites like D31N and E65Q.

Mutational effects on the ^{15}N HSQC spectrum of ^{15}N -Adx

While none of the surface mutations of ^{15}N -Adx were found to compromise the protein fold, certain substitutions were found to perturb the ^{15}N -HSQC spectra in different ways. For example, D72N, in the absence of any CYP, was found to induce only local changes in the amide signal for neighboring residues. Such “neighboring” effects, also observed for the E65Q mutation, are expected for substitution of a single side chain. In contrast, the mutant D31N, also in the absence of any CYP, was found to induce both local as well as longer range perturbations on more remote sites, specifically on residues Val-7 to His-10 on the first N-terminal β -strand and on residue Lys-98 of an adjacent loop (Supplemental Figure 5).

DMD # 87759

Recognition of ^{15}N -Adx by CYP24A1 in complex with 1,25(OH) $_2$ D3

In order to examine the influence of 1,25(OH) $_2$ D3 on formation of the Adx-CYP24A1 complex, we acquired HSQC spectra of ^{15}N -Adx samples containing incremental concentrations of substrate bound CYP24A1. In order to ensure that substrate does not directly affect the structure of Adx, we first overlaid spectra of ^{15}N -Adx with and without substrate and in the absence of CYP. For this control experiment, we identified a small number of up-field chemical shift perturbations corresponding to the N-terminal β -strands and the C-terminal domain of Adx. However, the effects were generally distributed away from the three α -helices near the iron and did not affect the peak intensity of the spectra. A subsequent comparison of ^{15}N -Adx with and without 1 α (OH)D3 produced what we interpret to be similar non-specific effects.

Interestingly, compared to the ligand free titration, addition of 0.2 molar equivalents of substrate bound CYP24A1 did not produce the same degree of overall peak broadening. Final peak intensities were approximately twice as high as those observed in the ligand-free state for the corresponding protein ratios. Upon further addition (0.4 molar equivalents), the substrate bound enzyme induced further broadening of the Adx spectrum, but still not to the same degree as observed with 0.2 molar equivalents of ligand free enzyme (Figure 4A, Supplemental Table 2, and Supplemental Figure 6). Despite this reduction in the net peak broadening, addition of 0.4 molar equivalents of substrate bound CYP24A1 induced a distribution of peak broadening on Adx that is more focused near α -helix 3 when compared to the pattern observed in the absence of substrate (Figure 5, left and center panels). More focused peak broadening near α -helix 3 also affects Leu-80, which has previously been reported as contributing a hydrophobic contact upon binding to CYP11B1 and CYP11B2 (Peng and Auchus, 2017).

DMD # 87759

1 α (OH)D3 disrupts specificity of the CYP24A1-Adx redox complex

In order to determine whether specificity of ligand binding influences recognition of Adx, we acquired a parallel set of ^{15}N -Adx spectra in the presence of incremental concentrations of CYP24A1 bound to the analog 1 α (OH)D3. Despite the absence of the carbon-25 hydroxyl (Figure 6), titration of CYP24A1 with the analog produces a standard type-I shift of the Soret band toward 392 nm. In general, spectral binding of 1 α (OH)D3 appears comparable to that of 1,25(OH) $_2$ D3, with each displaying sub- μM affinity. Here we observe that addition of CYP24A1 bound to 1 α (OH)D3 results in reduced net peak broadening (Figure 4B). However, samples containing additional CYP24A1 (0.4 molar equivalents) fail to promote further complex formation, likely indicating a fundamental change in molecular recognition of Adx. Moreover, a comparison of the resulting peak broadening on Adx in response to the presence of both vitamin-D ligands demonstrates a significant disruption of the pattern when CYP24A1 is bound to 1 α (OH)D3 (Figure 5, right panel, and Supplemental Figure 6). Notably, the differential effect on α -helix 3 is reduced, replaced by peak broadening that is distributed non-contiguously throughout the structure and affecting, among other sites, Leu-29 of α -helix 1, His-10 and Met-103 of the anterior β -strands, and His-62 of α -helix 2.

DMD # 87759

Cross-linking of the CYP24A1-Adx complex in the presence of 1,25(OH)₂D3 and 1 α (OH)D3

Independent of the pattern of NMR peak broadening for individual residues, the presence of either ligand reduced overall net broadening, consistent with a disruption of the redox complex (Figure 4). To evaluate this effect using a complementary approach, we carried out a series of chemical cross-linking experiments using the amine reactive linker EDC. EDC has previously been used to capture redox complexes between the mitochondrial CYP11B enzymes and Adx (Peng and Auchus, 2017). EDC treatment of CYP24A1 with Adx followed by electrophoresis produces a resolvable protein complex band at approximately 65 kDa (Figure 7A and Supplemental Figure 7). In order to draw a close comparison to the NMR data, the EDC reactions were carried out using identical protein ratios as those represented in the NMR data (1:0.2 and 1:0.4 for Adx:CYP24A1) and in the absence and presence of either ligand. Here we observe that there appear to be no significant differences between the cross-linking efficiency of the redox complex using CYP24A1 with or without ligand or bound to either 1,25(OH)₂D3 or 1 α (OH)D3 (Figure 7B). As a way to quantify a relative affinity between each redox complex, we also carried out EDC cross-linking at incrementally increasing concentrations of CYP24A1. The saturation curves, shown in separate panels in Figure 7C, indicate that the complex using unliganded CYP24A1 reaches a maximum at approximately 10 μ M CYP24A1 for samples containing 40 μ M Adx. We should note that accumulation of the covalently cross-linked product likely affects dissociation dynamics in a way that prevents measurement of full binding equilibria. However, the saturation curve suggests an apparent association constant (K_{on}) of approximately 1.5 μ M. This would be consistent with a binding constant for a protein interaction that displays the intermediate chemical exchange that we observe by NMR. Notably, addition of 1,25(OH)₂D3 and 1 α (OH)D3 produce similar saturation points, thus indicating that, as captured by chemical cross-linking, vitamin-D ligand does not induce a large change in binding affinity.

DMD # 87759

CYP24A1 activity in the presence of 1,25(OH)₂D₃ and 1 α (OH)D₃ results in similar production of H₂O₂

Production of H₂O₂ by way of a peroxide shunt is a well-documented by-product of CYP catalysis. In some cases, close coupling between reducing equivalents and productive catalysis is accompanied by a reduction in relative production of H₂O₂ (Peng et al., 2016), as more equivalents are routed to product formation. Here we anticipated that low CYP24A1 activity that results primarily from an unproductive orientation of substrate, and in which molecular recognition of the electron donor remains unaffected, would result in a proportional increase in the amount of reactive oxygen species produced as a result of unaltered electron delivery. As expected, in comparison to the biological substrate, there was minimal depletion of 1 α (OH)D₃ either at a 1:1 Adx to CYP24A1 ratio (Figure 8A) or at the ratios represented in the NMR titrations (Supplemental Figure 8). However, the amount of H₂O₂ measured for reactions with either substrate is very similar (Figure 8B), thus pointing toward a general disruption in electron delivery and consistent with a disruption in the specificity of the CYP24A1-Adx complex.

DMD # 87759

Discussion

Electron transfer by means of a protein interaction with Adx is essential for all reactions catalyzed by mitochondrial CYPs. We previously reported the investigation of clotrimazole-bound CYP24A1-Adx complexes using CYP isoforms from human, rat, and opossum, which show different regioselectivity for the hydroxylation of the vitamin-D side chain. The different complexes were also shown to rely on distinct secondary binding sites on Adx. While the previous study presented a correlation between regioselectivity and redox partner recognition, the use of inhibitor in lieu of vitamin-D ligand meant that subtle vitamin-D driven modulations of the redox complex were not accessible. In this study, we combine two-dimensional protein NMR EDC cross-linking, mutagenesis, and functional assays to compare the CYP24A1, Adx complex in the absence of ligand and in the presence of biological substrate 1,25(OH)₂D₃, as well as the supplement 1 α (OH)D₃. In order to remove potential ambiguities from non-conserved species variation of the protein surfaces, we focused entirely on CYP24A1 and Adx from rat, a carbon-24 hydroxylase system.

In the ligand free state, rat CYP24A1 was found to induce modest differential peak broadening on the HSQC spectra of ¹⁵N-Adx (Figure 2), with a pattern that points toward α -helix 3 as the principle recognition site. This finding is consistent with prior identification of α -helix 3 as a key CYP binding site (Bureik et al., 2005; Heinz et al., 2005; Strushkevich et al., 2011; Peng et al., 2016). Furthermore, similar to what we reported for the mixed-species complexes, disruption of the interaction by point mutations outside of α -helix 3 suggests a role for auxiliary contributions from secondary sites, potentially via modulation of the Adx dimer interface. The oxidized form of Adx is known to self-associate into dimers (Pikuleva et al., 2000; Behlke et al., 2007). Among the mutants we generated in rat Adx, D31N is a candidate for involvement in the dimer interface due to the intermediate and long-range chemical shift perturbations of the mutant ¹⁵N-HSQC spectrum (Figures S4 and S5).

DMD # 87759

Substrate-driven modulations of the protein interactions between CYPs and accessory proteins have previously been reported as a form of regulatory control in the non-mitochondrial CYP enzymes (Estrada et al., 2013; Estrada et al., 2014; Bart and Scott, 2017). A salient example is the steroid metabolizing and multifunctional enzyme CYP17A1, which receives electrons from either a P450 oxidoreductase (CPR) or the modulator protein cytochrome b_5 (b_5). Since CPR and b_5 bind on overlapping surfaces on the proximal side of CYP17A1, the interaction is competitive, with particular CYP17A1 substrates modulating the respective affinities between the redox complexes in a way that correlates with modulation of each reaction (Peng et al., 2016; Duggal et al., 2018). Another example with a more closely related electron delivery scheme to that of mitochondrial CYPs is bacterial P450cam, which binds its cognate redox partner putidaredoxin with a higher affinity when bound to substrate (Hollingsworth et al., 2016).

In order to determine the relevance of similar substrate or ligand driven effects as a component of modulating CYP24A1 function, we incorporated both 1,25(OH)₂D3 as well as the supplement 1 α (OH)D3 into the NMR protein binding assays. 1 α (OH)D3 bypasses metabolism by the 1 α -hydroxylase CYP27B1 and is instead rapidly converted into 1,25(OH)₂D3 in liver (Gallacher et al., 1994). Despite having a high affinity for CYP24A1, reconstituted CYP24A1 assays show 1 α (OH)D3 to be a poor substrate, with turnover rates of less than 5% of those observed with 1,25(OH)₂D3 (Kaufmann 2011). More broadly, modification of the aliphatic side chain in vitamin-D analogs is generally known to reduce catabolism by CYP24A1. For instance, the analogs EB 1089 and 20-epi-1,25(OH)₂D3 behave as superagonists in part due to their sustained metabolic stability (Kissmeyer et al., 1997; Zella et al., 2009; Leyssens et al., 2014).

DMD # 87759

Here we find that addition of 1,25(OH)₂D₃ promotes a more focused pattern of peak broadening on α -helix 3 of Adx (Figure 5), consistent with an increase in the specificity of the protein complex than was observed without ligand. In contrast, addition of 1 α (OH)D₃ results in disruption of peak broadening, with differential effects distributed on non-contiguous surfaces. We interpret this effect to represent a loss in the specificity of the interaction, with the redox partners likely sampling multiple orientations when bound to the analog. Loss of specificity is also supported by the observation that the addition of increasing concentrations of CYP24A1 bound to 1 α (OH)D₃ does not appear to induce further complex formation (Figure 4B). These findings, along with a likely disruption of the functional redox complex (Figure 8), suggest that proper substrate binding and orientation are necessary for optimal recognition of the electron donor. Furthermore, it underscores the importance of the carbon-25 hydroxyl in substrate orientation in the CYP24A1 active site.

An unexpected finding in this study was the apparent decrease in the relative amount of complex formed between Adx and CYP24A1 bound to 1,25(OH)₂D₃. This finding is reflected in a 1D spectrum of residue Glu-73 (located on the interaction site of Adx) in Figure 4A and in the net summary of line broadening shown in Figure 4B. The implication is that substrate binding appears to reduce the affinity for the electron donor. This outcome stands in contrast to similar NMR studies involving other (non-mitochondrial) CYP-redox partner interactions, in which substrate leads to enhanced overall peak broadening (Estrada et al., 2013; Zhang et al., 2015; Bart and Scott, 2017). In order to verify these effects using a complementary technique, we also carried out a series of EDC chemical cross-linking analyses in which we found no significant difference in cross-linking efficiency between the vitamin-D bound and ligand-free CYP24A1-Adx complexes. This was in clear contrast to the NMR data, which indicated a ligand-induced loss in the complex. It should be noted, however, that covalent cross-linking and accumulation of the complex may impact binding equilibria in a way that masks small

DMD # 87759

differences in affinity. It should also be noted that a theoretical change in CYP-Adx affinity, in particular where multiple recognition sites are involved, might occur independent of changes in functional specificity of the complex. Put another way, changes in ligand-induced specificity, as suggested by mapping the NMR effects in this study, may or may not be accompanied by changes in protein-protein affinity. Nevertheless, with consideration that substrate-induced changes in CYP protein-protein interactions are known to occur in microsomal CYPs, further investigation of substrate-induced changes in mitochondrial CYPs is warranted.

In summary, these findings provide structural evidence of substrate-induced modulation of the CYP24A1 redox-binding surface, as represented by differential NMR peak broadening of the Adx surface. This feature of CYP function has not previously been demonstrated for a mitochondrial member of the CYP family. With respect to vitamin-D metabolism, these findings also provide evidence that the specificity of vitamin-D recognition, particularly as determined by the carbon-25 hydroxyl of 1,25(OH)₂D₃, also confers specificity to the CYP24A1-Adx interaction. More broadly, this work also provides a structural basis for low substrate turnover of side-chain modified vitamin-D analogs.

DMD # 87759

Acknowledgements:

The authors would like to thank Dr. Richard Browne and Sonia Bhattacharya from the Department of Biotechnical and Clinical Laboratory Sciences, University at Buffalo, for their assistance in optimizing the preparation of vitamin-D liquid chromatography samples used to resolve vitamin-D substrates.

Conflict of Interest statement: The authors have no conflict of interest to declare.

DMD # 87759

Authorship Contributions:

Participated in research design: Kumar and Estrada

Conducted experiments: Kumar

Performed data analysis: Kumar

Wrote or contributed to the writing of the manuscript: Kumar and Estrada

DMD # 87759

References:

- Bart AG and Scott EE (2017) Structural and functional effects of cytochrome b5 interactions with human cytochrome P450 enzymes. *J Biol Chem* **292**:20818-20833.
- Bax A and Ikura M (1991) An efficient 3D NMR technique for correlating the proton and 15N backbone amide resonances with the alpha-carbon of the preceding residue in uniformly 15N/13C enriched proteins. *J Biomol NMR* **1**:99-104.
- Beckman MJ, Tadikonda P, Werner E, Prahl J, Yamada S, and DeLuca HF (1996) Human 25-hydroxyvitamin D3-24-hydroxylase, a multicatalytic enzyme. *Biochemistry* **35**:8465-8472.
- Behlke J, Ristau O, Muller EC, Hannemann F, and Bernhardt R (2007) Self-association of adrenodoxin studied by using analytical ultracentrifugation. *Biophys Chem* **125**:159-165.
- Bureik M, Zollner A, Schuster N, Montenarh M, and Bernhardt R (2005) Phosphorylation of bovine adrenodoxin by protein kinase CK2 affects the interaction with its redox partner cytochrome P450_{scc} (CYP11A1). *Biochemistry* **44**:3821-3830.
- Constantine KL, Goldfarb V, Wittekind M, Friedrichs MS, Anthony J, Ng SC, and Mueller L (1993) Aliphatic 1H and 13C resonance assignments for the 26-10 antibody VL domain derived from heteronuclear multidimensional NMR spectroscopy. *J Biomol NMR* **3**:41-54.
- Delaglio F, Grzesiek S, Vuister GW, Zhu G, Pfeifer J, and Bax A (1995) NMRPipe: a multidimensional spectral processing system based on UNIX pipes. *J Biomol NMR* **6**:277-293.
- Duggal R, Denisov IG, and Sligar SG (2018) Cytochrome b5 enhances androgen synthesis by rapidly reducing the CYP17A1 oxy-complex in the lyase step. *FEBS Lett* **592**:2282-2288.
- Estrada DF (2018) The cytochrome P450 24A1 interaction with adrenodoxin relies on multiple recognition sites that vary among species. *J Biol Chem* **293**:4167-4179.
- Estrada DF, Laurence JS, and Scott EE (2013) Substrate-modulated cytochrome P450 17A1 and cytochrome b5 interactions revealed by NMR. *J Biol Chem* **288**:17008-17018.
- Estrada DF, Skinner AL, Laurence JS, and Scott EE (2014) Human Cytochrome P450 17A1 Conformational Selection: Modulation by Ligand and Cytochrome b5. *J Biol Chem*.
- Ewen KM, Kleser M, and Bernhardt R (2011) Adrenodoxin: the archetype of vertebrate-type [2Fe-2S] cluster ferredoxins. *Biochim Biophys Acta* **1814**:111-125.
- Gallacher SJ, Cowan RA, Fraser WD, Logue FC, Jenkins A, and Boyle IT (1994) Acute effects of intravenous 1 alpha-hydroxycholecalciferol on parathyroid hormone, osteocalcin and calcitriol in man. *Eur J Endocrinol* **130**:141-145.
- Grzesiek S, Dobeli H, Gentz R, Garotta G, Labhardt AM, and Bax A (1992) 1H, 13C, and 15N NMR backbone assignments and secondary structure of human interferon-gamma. *Biochemistry* **31**:8180-8190.
- Grzesiek S, Vuister GW, and Bax A (1993) A simple and sensitive experiment for measurement of JCC couplings between backbone carbonyl and methyl carbons in isotopically enriched proteins. *J Biomol NMR* **3**:487-493.
- Hamamoto H, Kusudo T, Urushino N, Masuno H, Yamamoto K, Yamada S, Kamakura M, Ohta M, Inouye K, and Sakaki T (2006) Structure-function analysis of vitamin D 24-hydroxylase (CYP24A1) by site-directed mutagenesis: amino acid residues responsible for species-based difference of CYP24A1 between humans and rats. *Mol Pharmacol* **70**:120-128.
- Heinz A, Hannemann F, Muller JJ, Heinemann U, and Bernhardt R (2005) The interaction domain of the redox protein adrenodoxin is mandatory for binding of the electron acceptor CYP11A1, but is not required for binding of the electron donor adrenodoxin reductase. *Biochem Biophys Res Commun* **338**:491-498.
- Holick MF (2007) Vitamin D deficiency. *The New England journal of medicine* **357**:266-281.
- Hollingsworth SA, Batabyal D, Nguyen BD, and Poulos TL (2016) Conformational selectivity in cytochrome P450 redox partner interactions. *Proceedings of the National Academy of Sciences of the United States of America* **113**:8723-8728.

DMD # 87759

- Johnson BA (2004) Using NMRView to visualize and analyze the NMR spectra of macromolecules. *Methods in molecular biology* **278**:313-352.
- Kaufmann M, Prosser DE, and Jones G (2011) Bioengineering anabolic vitamin D-25-hydroxylase activity into the human vitamin D catabolic enzyme, cytochrome P450 CYP24A1, by a V391L mutation. *J Biol Chem* **286**:28729-28737.
- Kissmeyer AM, Binderup E, Binderup L, Mork Hansen C, Andersen NR, Makin HL, Schroeder NJ, Shankar VN, and Jones G (1997) Metabolism of the vitamin D analog EB 1089: identification of in vivo and in vitro liver metabolites and their biological activities. *Biochem Pharmacol* **53**:1087-1097.
- Kostic M, Pochapsky SS, Obenauer J, Mo H, Pagani GM, Pejchal R, and Pochapsky TC (2002) Comparison of functional domains in vertebrate-type ferredoxins. *Biochemistry* **41**:5978-5989.
- Laskowski RA, Rullmannn JA, MacArthur MW, Kaptein R, and Thornton JM (1996) AQUA and PROCHECK-NMR: programs for checking the quality of protein structures solved by NMR. *J Biomol NMR* **8**:477-486.
- Leysens C, Verlinden L, and Verstuyf A (2014) The future of vitamin D analogs. *Front Physiol* **5**:122.
- Peng HM and Auchus RJ (2017) Molecular Recognition in Mitochondrial Cytochromes P450 That Catalyze the Terminal Steps of Corticosteroid Biosynthesis. *Biochemistry* **56**:2282-2293.
- Peng HM, Im SC, Pearl NM, Turcu AF, Rege J, Waskell L, and Auchus RJ (2016) Cytochrome b5 Activates the 17,20-Lyase Activity of Human Cytochrome P450 17A1 by Increasing the Coupling of NADPH Consumption to Androgen Production. *Biochemistry* **55**:4356-4365.
- Pikuleva IA, Tesh K, Waterman MR, and Kim Y (2000) The tertiary structure of full-length bovine adrenodoxin suggests functional dimers. *Archives of biochemistry and biophysics* **373**:44-55.
- Prosser DE, Kaufmann M, O'Leary B, Byford V, and Jones G (2007) Single A326G mutation converts human CYP24A1 from 25-OH-D3-24-hydroxylase into -23-hydroxylase, generating 1 α ,25-(OH)₂D₃-26,23-lactone. *Proceedings of the National Academy of Sciences of the United States of America* **104**:12673-12678.
- Ryan JW, Anderson PH, Turner AG, and Morris HA (2013) Vitamin D activities and metabolic bone disease. *Clin Chim Acta* **425**:148-152.
- Siu-Caldera ML, Zou L, Ehrlich MG, Schwartz ER, Ishizuka S, and Reddy GS (1995) Human osteoblasts in culture metabolize both 1 α , 25-dihydroxyvitamin D₃ and its precursor 25-hydroxyvitamin D₃ into their respective lactones. *Endocrinology* **136**:4195-4203.
- Strushkevich N, MacKenzie F, Cherkesova T, Grabovec I, Usanov S, and Park HW (2011) Structural basis for pregnenolone biosynthesis by the mitochondrial monooxygenase system. *Proceedings of the National Academy of Sciences of the United States of America* **108**:10139-10143.
- Waterhouse A, Bertoni M, Bienert S, Studer G, Tauriello G, Gumienny R, Heer FT, de Beer TAP, Rempfer C, Bordoli L, Lepore R, and Schwede T (2018) SWISS-MODEL: homology modelling of protein structures and complexes. *Nucleic Acids Res* **46**:W296-W303.
- Weiss R, Brachais L, Lohr F, Hartleib J, Bernhardt R, and Ruterjans H (2000) Assignment of 1H, 13C and 15N signals of bovine adrenodoxin. *J Biomol NMR* **17**:355-356.
- Weissgerber TL, Savic M, Winham SJ, Stanisavljevic D, Garovic VD, and Milic NM (2017) Data visualization, bar naked: A free tool for creating interactive graphics. *J Biol Chem* **292**:20592-20598.
- Wishart DS and Sykes BD (1994) The 13C chemical-shift index: a simple method for the identification of protein secondary structure using 13C chemical-shift data. *J Biomol NMR* **4**:171-180.
- Yang J, Yan R, Roy A, Xu D, Poisson J, and Zhang Y (2015) The I-TASSER Suite: protein structure and function prediction. *Nat Methods* **12**:7-8.

DMD # 87759

- Zella LA, Meyer MB, Nerenz RD, and Pike JW (2009) The enhanced hypercalcemic response to 20-epi-1,25-dihydroxyvitamin D3 results from a selective and prolonged induction of intestinal calcium-regulating genes. *Endocrinology* **150**:3448-3456.
- Zhang M, Le Clair SV, Huang R, Ahuja S, Im SC, Waskell L, and Ramamoorthy A (2015) Insights into the role of substrates on the interaction between cytochrome b5 and cytochrome P450 2B4 by NMR. *Scientific reports* **5**:8392.

DMD # 87759

Footnotes

This work was supported by the National Institutes of Health, Institute of General Medical Sciences, grant number [R00GM112862 (DFE)].

DMD # 87759

Figure Legends:

Figure 1. Assigned ^{15}N -HSQC spectrum of oxidized full-length rat Adx.

Figure 2. Mapping of differential peak broadening of ^{15}N -Adx. A) The structure of Adx was modeled based on the secondary chemical shift index. Regions that undergo differential peak broadening as a result of titration with 0.2 molar equivalents ligand free CYP24A1 are indicated by red (1 std.dev.) and orange (0.75 std.dev.). B) Corresponding peak broadening for all assigned residues, with the mean ratio indicated by the dashed line.

Figure 3. Effect of charge-neutralizing mutations on peak broadening of ^{15}N -Adx. A) Point substitutions designed to neutralize surface charges on Adx perturb the CYP24A1 induced peak-broadening pattern to varying extents as compared to wild-type protein. Differentially broadened residues are selected based on one and 0.75 standard deviations from the mean for a 1:0.2 molar ratio of ^{15}N -Adx: ligand free CYP24A1. B) Net per residue peak broadening for the interaction with ligand free CYP24A1 is reflected in box plots in which remaining intensities for individual residues are represented by each data point, suggesting that mutations D31N, E65Q, and D72N all reduce the extent of the redox complex formation.

Figure 4. Ligand-induced modulation of CYP24A1-Adx complex. NMR data of the complex acquired in the presence of 1,25(OH)₂D3 reflects a relative reduction in peak broadening, as indicated by the 1D spectrum of Glu-73 in (A). The effect of 1,25(OH)₂D3 or 1 α (OH)D3 on the net loss of peak broadening is summarized in (B) in which remaining intensities for individual residues are represented by each data point in the box plots.

DMD # 87759

Figure 5. Mapping of the ligand-induced modulation of the CYP24A1-Adx complex.

Mapping the most affected regions on the structure of rat Adx reflects a focusing on α -helix 3 when in the presence of $1,25(\text{OH})_2\text{D}_3$ (center panel), relative to the ligand-free interaction (left panel). In contrast, the complex in the presence of $1\alpha(\text{OH})\text{D}_3$ becomes non-specific, as indicated by increased distribution of peak broadening (right panel).

Figure 6. Spectral binding assays for CYP24A1 vitamin D ligands.

Titration of $1,25(\text{OH})_2\text{D}_3$ and $1\alpha(\text{OH})\text{D}_3$ (A) induce similar high-spin shifts of the Soret band of rat CYP24A1 (B) and bind with similar sub- μM affinity. Error bars reflect binding data acquired in triplicate and the K_d calculated error reflects the quality of fit to a hyperbolic binding curve. Error bars for the titration of $1\alpha(\text{OH})\text{D}_3$ are smaller than the data icons.

Figure 7. EDC chemical cross-linking of the CYP24A1-Adx complex.

(A) Incubation with EDC results in a CYP24A1-Adx cross-linked product of approximately 65 kDa, consistent with a 1:1 complex. In order to examine cross-linking of the complex with ligand-induced disruption of the complex as observed by NMR, cross-linking was carried out using identical protein ratios as the NMR samples (B), in which the presence of ligand does not appear to disrupt the efficiency of cross-linking. Lastly, CYP24A1 titrations of the complex as quantified by gel electrophoresis histograms are shown in (C), in which the apparent association constant of the complex is not affected by the presence of vitamin-D ligand.

DMD # 87759

Figure 8. CYP24A1 depletion of 1,25(OH)₂D₃ and 1α(OH)D₃. Vitamin-D compound depletion was carried out by reconstituted CYP24A1 assays. As expected, 1α(OH)D₃ is minimally depleted in comparison with 1,25(OH)₂D₃ for a corresponding 5 minute reaction time. However, the amount of H₂O₂ produced over the same time period is similar to that measured with the biological substrate.

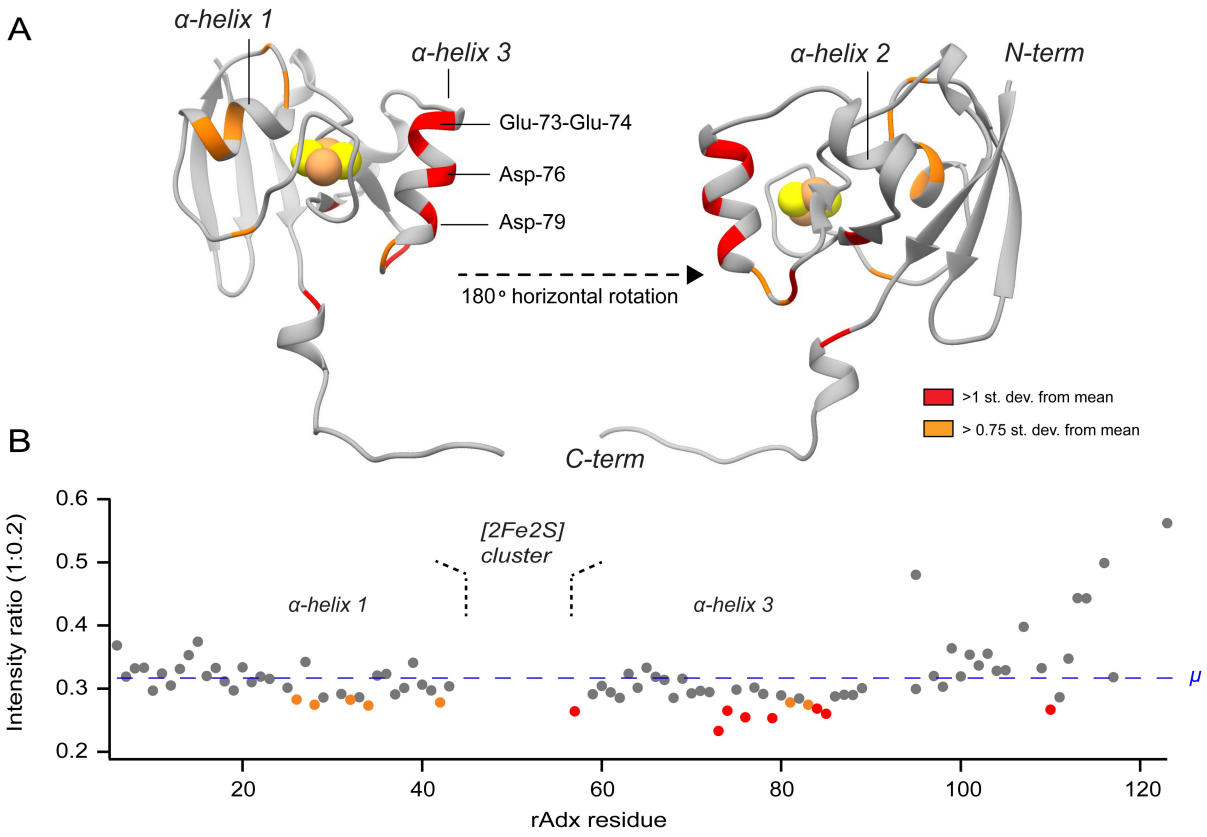


Figure 2

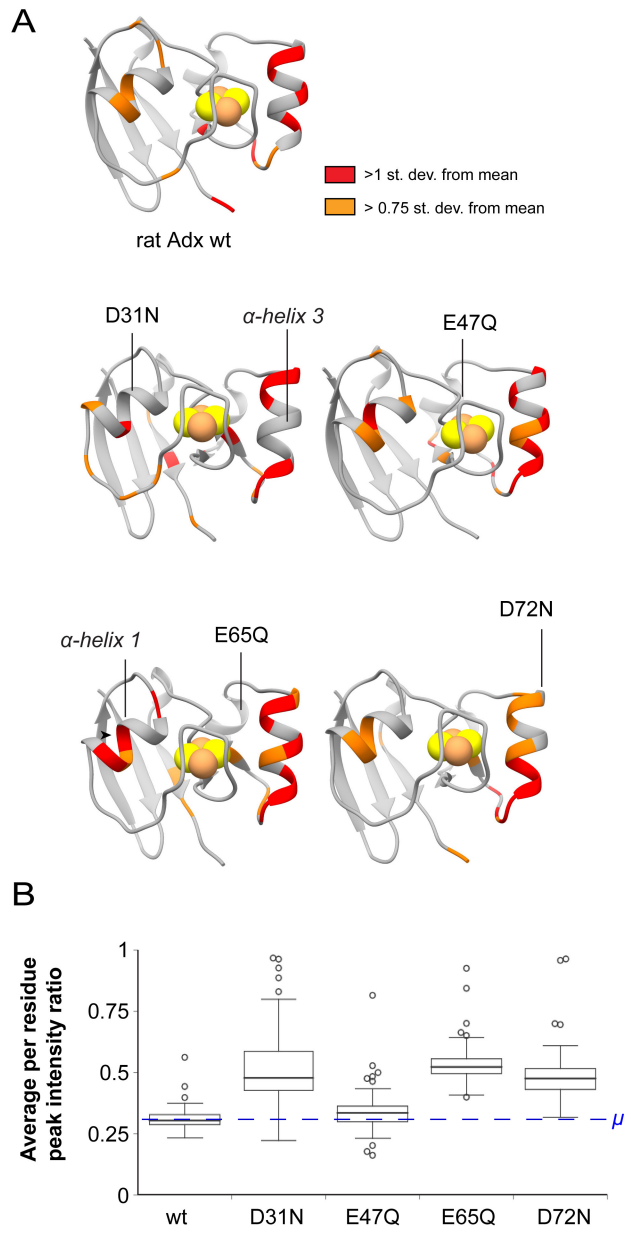


Figure 3

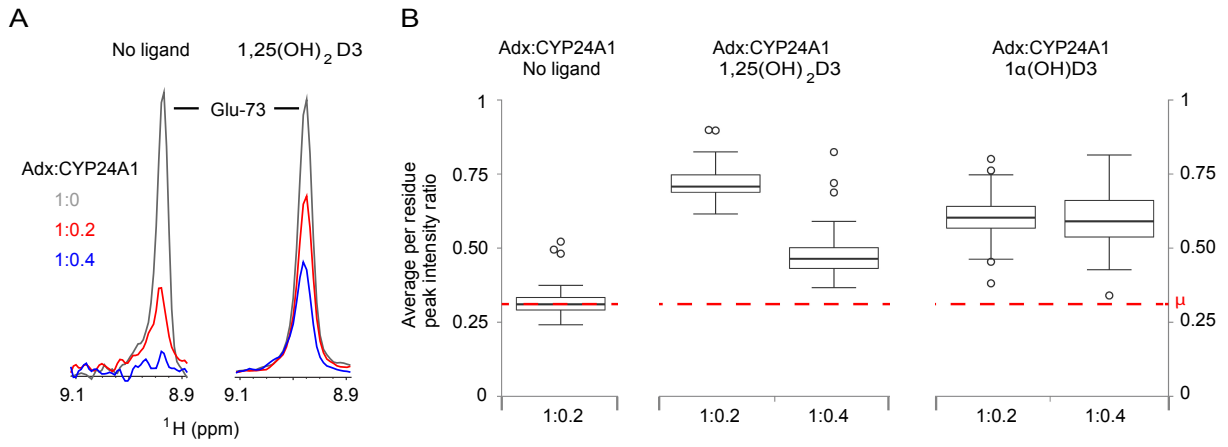


Figure 4

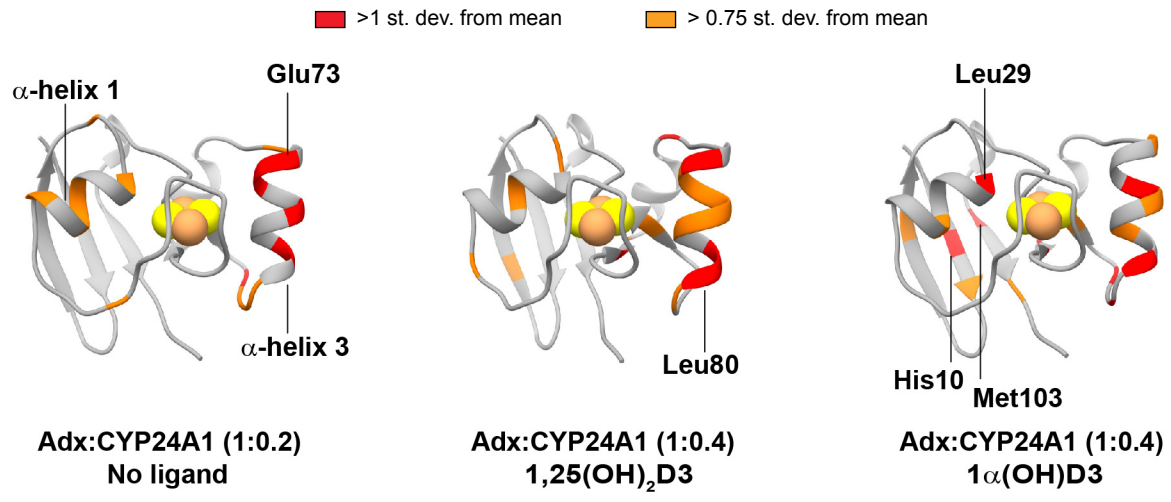


Figure 5.

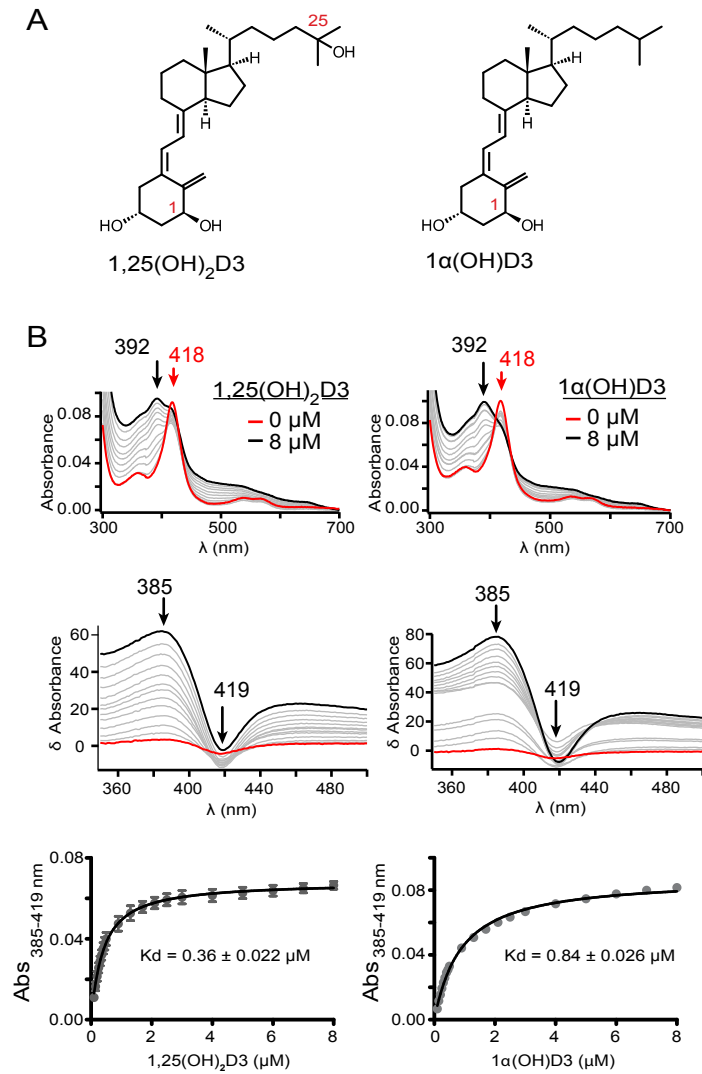


Figure 6.

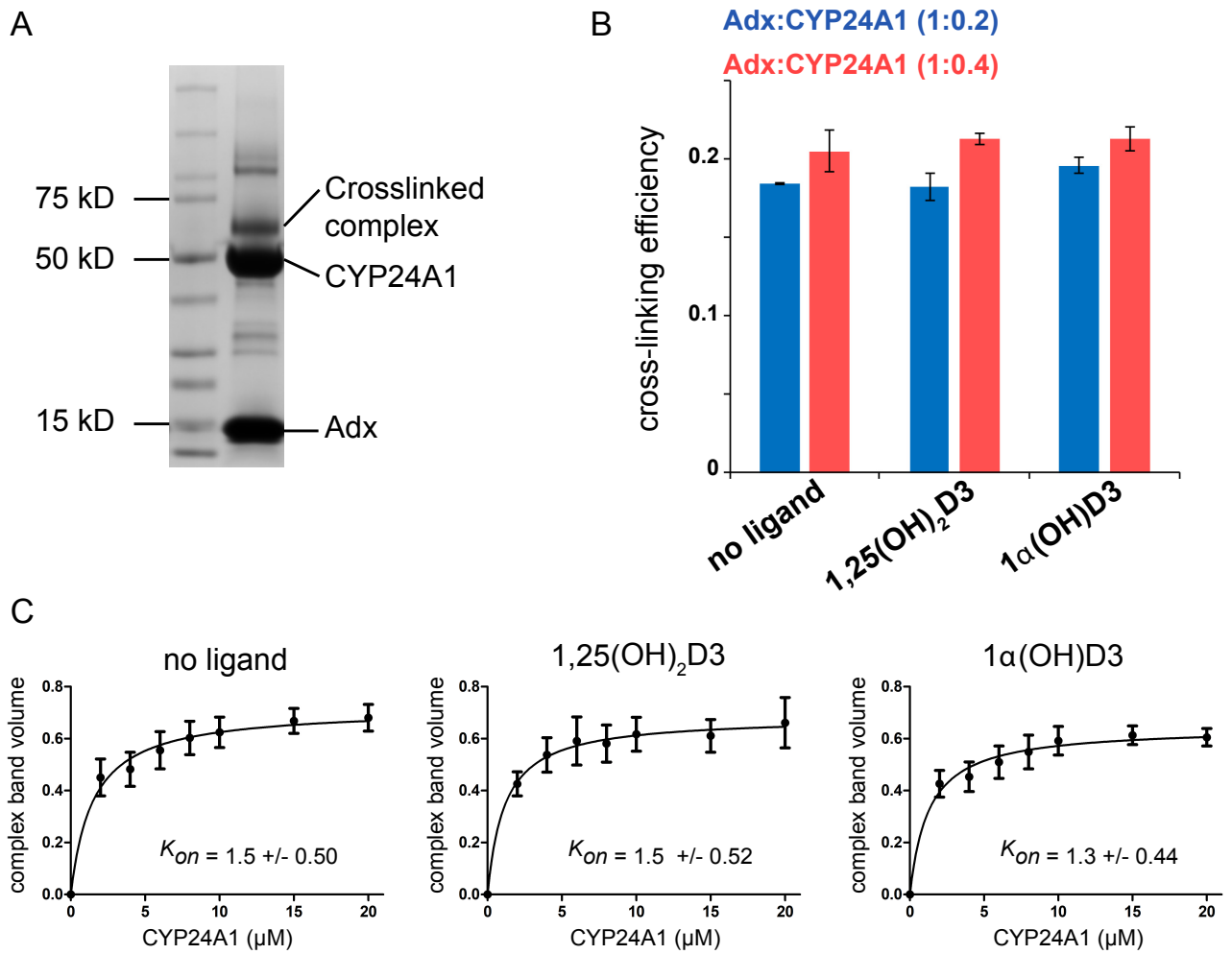


Figure 7.

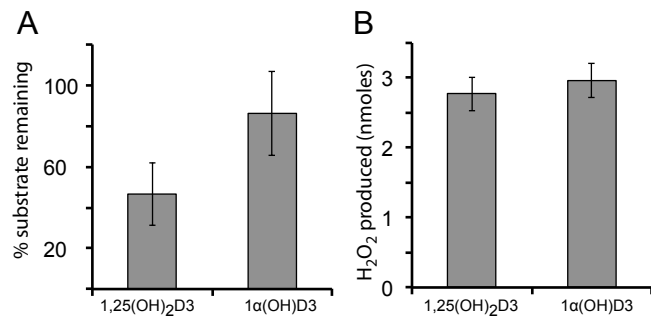


Figure 8.

Supplemental Tables and Figures:

Specificity of the redox complex between cytochrome P450 24A1 and adrenodoxin relies on carbon-25 hydroxylation of vitamin-D substrate

Amit Kumar¹ & D. Fernando Estrada¹

Department of Biochemistry, Jacobs School of Medicine and Biomedical
Science, University at Buffalo, Buffalo NY 14203

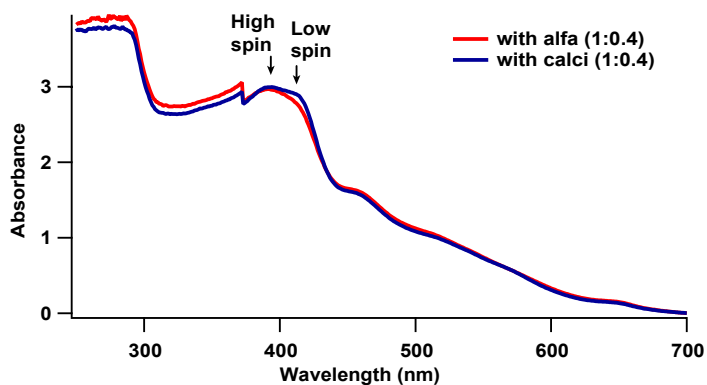


Figure S1. Absorption spectra of ^{15}N -Adx, CYP24A1 NMR samples following data acquisition. Both samples retained approximately equal concentrations of high spin (ligand bound) and low spin (ligand free) populations for the duration of data collection. $1,25(\text{OH})_2\text{D}_3$ bound spectrum is in blue and $1\alpha(\text{OH})\text{D}_3$ bound spectrum is in red.

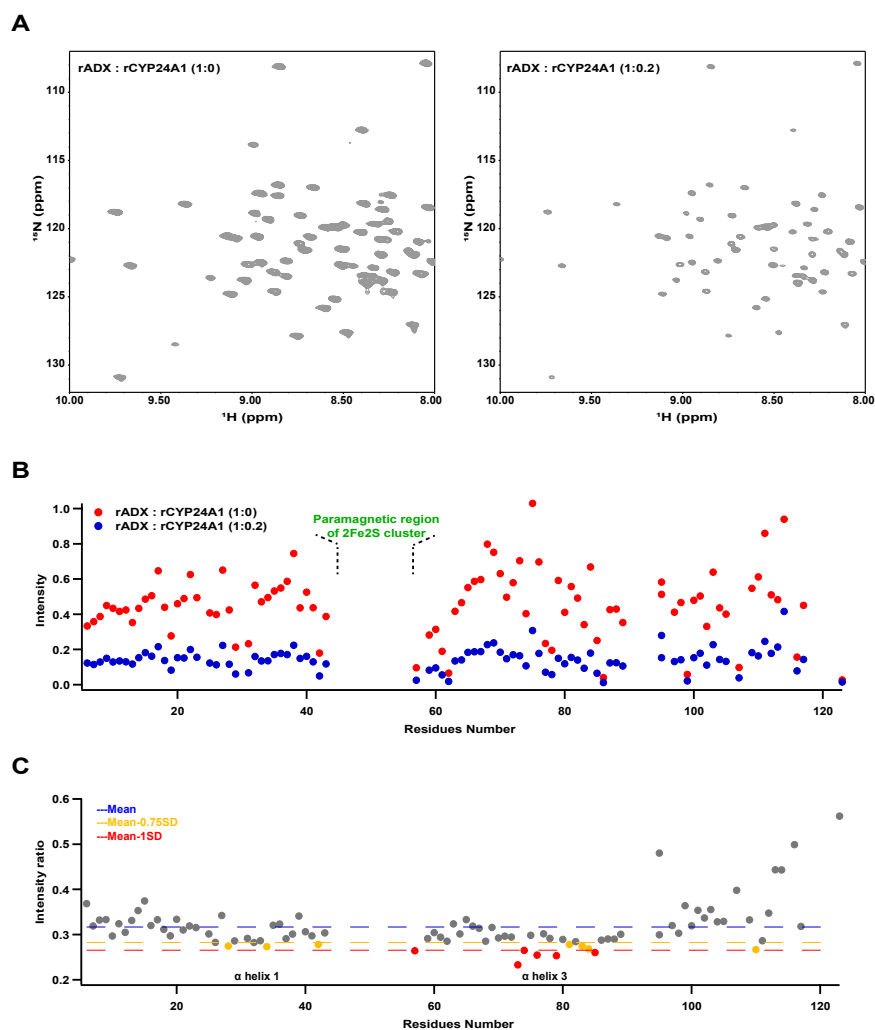


Figure S3. Line broadening effects induced by addition of ligand free CYP24A1. A) Excerpts of ^{15}N -HSQC spectra in the absence (left) and presence (right) of 0.2 molar equivalents of CYP24A1. Both spectra are displayed at the same contour levels. B) Scatter plot of the raw peak intensities induced by the protein-protein interaction. C) Final ratios reflecting signal intensity remaining, with disproportionately affected sites indicated in orange (more than 0.75 standard deviation from the mean) and red (more than 1 standard deviation from the mean). The blue line represents the mean ratio for all rat Adx residues.

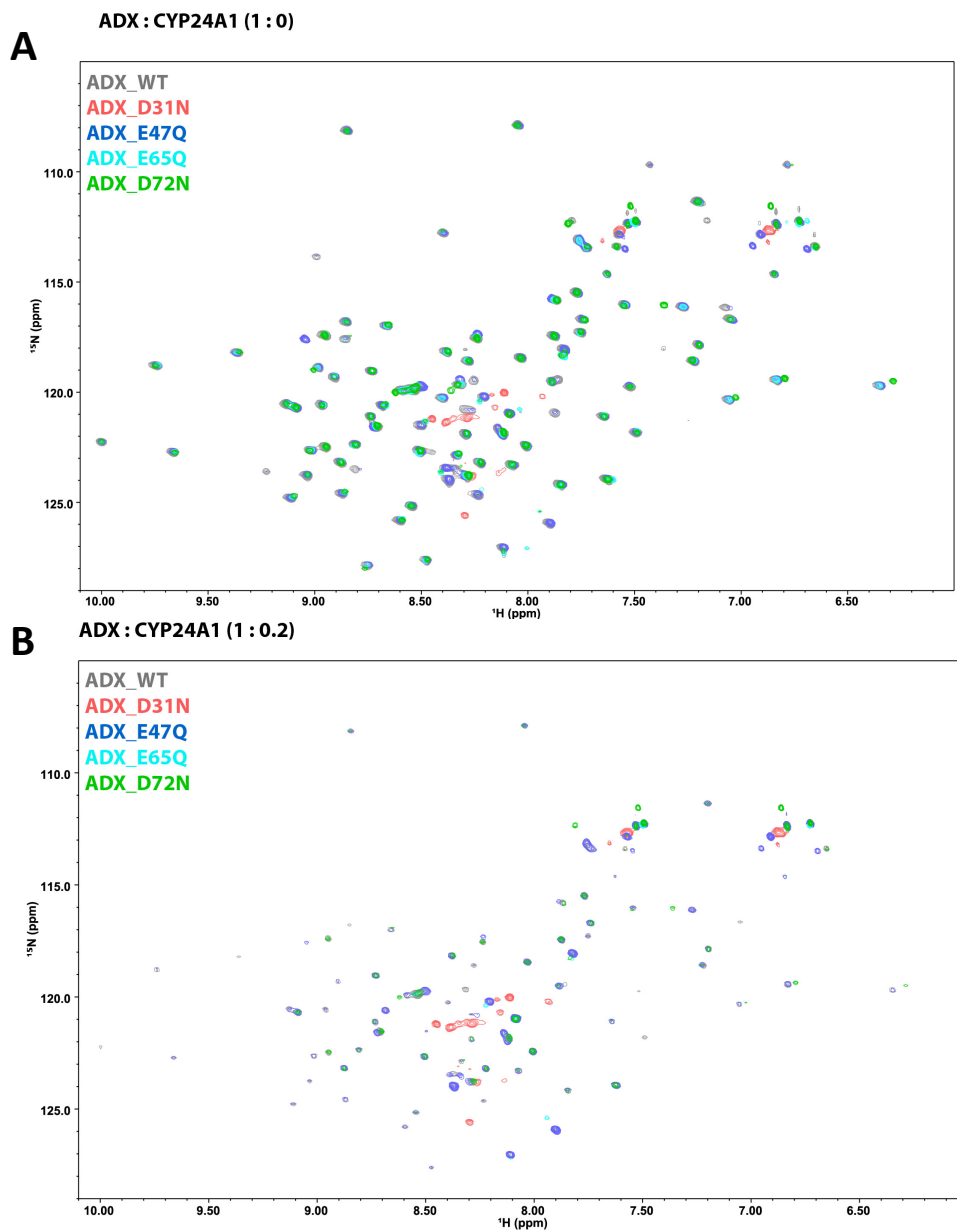


Figure S4. Overlay of CYP24A1-free and CYP24A1-bound ^{15}N -Adx mutant spectra. A) the 2D HSQC spectra of unbound mutant Adx are overlaid with wild-type Adx, in which the native fold of Adx is preserved for all point mutations. B) The same 2D HSQC spectra are shown in the presence of 0.2 equivalents of unlabeled, ligand-free CYP24A1.

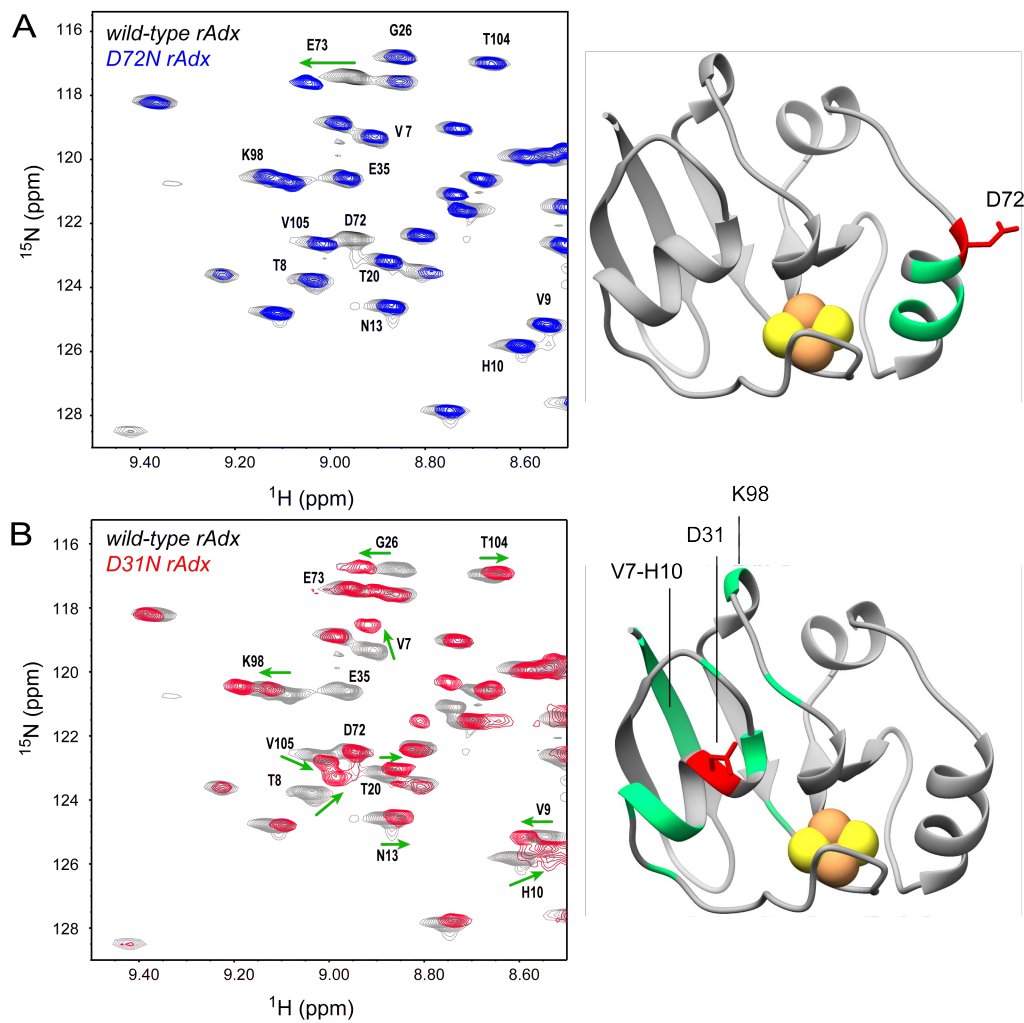


Figure S5. Mutagenesis induced chemical shift perturbations of ^{15}N -Adx.

The effect on the ^{15}N -Adx HSQC spectrum from single residue mutations D72N (A), in which only adjacent residues are affected, and D31N (B), in which non-local perturbations are observed. All spectra are displayed at equivalent contour levels.

Table S1. Remaining peak intensity ratios (from free ^{15}N -rAdx) of mutant ^{15}N -Adx with 0.2 molar equivalents of CYP24A1. Resonances are broadened more than 0.75 standard deviations (orange) or more than 1 full standard deviation (red) from the mean.

ADX WT		ADX D31N		ADX E47Q		ADX E65Q		ADX D72N	
E73	0.233	V33	0.222	E73	0.162	E73	0.399	L78	0.317
D79	0.253	E73	0.260	D76	0.177	D79	0.408	T85	0.324
D76	0.255	L80	0.263	L80	0.202	D76	0.414	L84	0.347
T85	0.260	D72	0.314	V32	0.231	V32	0.416	D79	0.353
L57	0.264	A81	0.333	E74	0.236	A81	0.419	A81	0.353
E74	0.265	E74	0.337	A81	0.236	S28	0.423	F82	0.361
A110	0.267	V105	0.344	D79	0.238	E74	0.433	L80	0.372
L84	0.268	R89	0.354	F59	0.246	L80	0.435	E73	0.387
I34	0.273	F59	0.355	T85	0.250	I34	0.441	V33	0.390
G83	0.275	E35	0.371	G26	0.253	V33	0.446	M77	0.390
S28	0.275	N86	0.376	M77	0.256	L84	0.457	E74	0.392
G42	0.278	L84	0.388	L57	0.257	V107	0.460	A110	0.394
A81	0.278	D41	0.388	L29	0.258	V105	0.464	V32	0.398
V32	0.283	L38	0.389	V33	0.261	T85	0.464	R89	0.399
G26	0.283	E109	0.394	I34	0.263	D72	0.467	N102	0.402
F82	0.284	F43	0.402	G83	0.267	M77	0.468	T71	0.403
D68	0.285	N102	0.402	L78	0.268	R89	0.469	G83	0.406
H62	0.285	H10	0.420	E60	0.271	E60	0.479	I34	0.410
L29	0.286	S88	0.421	S28	0.291	D68	0.491	E60	0.423
V33	0.286	G26	0.423	T71	0.297	K98	0.492	S28	0.425
V111	0.286	D39	0.426	L84	0.297	F82	0.493	D76	0.427
N86	0.288	T85	0.428	N37	0.299	D41	0.497	L19	0.432
L80	0.289	T21	0.429	R89	0.299	G83	0.501	E109	0.435
S88	0.290	L57	0.429	Y64	0.303	A110	0.501	F59	0.437
R87	0.290	E60	0.430	D72	0.304	L38	0.502	S117	0.438
N37	0.291	E65	0.431	K98	0.305	S117	0.505	I70	0.438
F59	0.291	D68	0.433	S88	0.309	T71	0.505	E35	0.440
D31	0.291	N75	0.436	F82	0.309	L78	0.506	L57	0.441
L78	0.292	T104	0.440	E35	0.313	E35	0.508	D41	0.442
I70	0.293	N13	0.440	T104	0.315	H10	0.511	S88	0.442
D61	0.294	K98	0.444	G42	0.318	T21	0.512	R14	0.445
D72	0.294	T20	0.449	L38	0.319	R14	0.512	K12	0.446
T71	0.297	I40	0.449	K12	0.322	D27	0.512	Y64	0.449
H10	0.297	K22	0.452	N102	0.325	T97	0.513	L38	0.450
D41	0.297	V32	0.454	D68	0.325	L19	0.513	T97	0.453
N75	0.298	I63	0.469	R87	0.327	A69	0.515	I63	0.454

R89	0.301	F11	0.471	D27	0.327	S88	0.515	T21	0.458
L38	0.301	D76	0.472	E109	0.327	F43	0.517	R87	0.462
V25	0.301	D61	0.473	T8	0.329	L57	0.519	F43	0.466
Y64	0.301	Y64	0.476	V9	0.331	V9	0.520	D31	0.467
M77	0.302	M77	0.476	L19	0.334	L29	0.521	M100	0.472
K98	0.303	M103	0.478	S117	0.334	I70	0.523	G26	0.475
F43	0.304	T8	0.488	G23	0.335	Y64	0.523	F11	0.476
E60	0.304	D15	0.489	M100	0.335	N37	0.524	N75	0.478
K12	0.305	L19	0.493	D61	0.336	T104	0.525	N13	0.480
I40	0.306	G23	0.501	H10	0.336	L67	0.525	T8	0.482
T21	0.310	R87	0.503	T97	0.336	N75	0.528	T104	0.483
T18	0.312	K12	0.514	D41	0.340	G26	0.531	D61	0.484
L67	0.314	V107	0.518	D39	0.340	R87	0.532	L29	0.486
G23	0.316	V7	0.519	L67	0.342	N36	0.535	L67	0.487
A69	0.316	D79	0.522	V105	0.342	I40	0.536	G42	0.490
S117	0.318	L67	0.523	F11	0.343	I63	0.537	H10	0.491
K66	0.319	T18	0.531	F43	0.344	N102	0.538	V105	0.491
V7	0.319	D27	0.536	I70	0.344	M103	0.540	A69	0.493
K22	0.319	L78	0.547	D31	0.344	M100	0.542	D101	0.494
M100	0.319	G83	0.549	A110	0.348	K12	0.543	D27	0.498
T97	0.320	M100	0.553	T20	0.351	N13	0.549	K98	0.507
G16	0.320	V9	0.562	A69	0.352	G16	0.549	M103	0.507
E35	0.321	A69	0.563	T21	0.353	T20	0.549	N36	0.508
L19	0.323	E17	0.569	N36	0.355	E109	0.552	V9	0.508
N36	0.323	K6	0.573	N13	0.357	F59	0.554	K66	0.510
I63	0.324	G16	0.583	I40	0.357	K22	0.555	V111	0.514
F11	0.324	N37	0.590	I63	0.357	V25	0.555	G23	0.514
T104	0.328	S28	0.592	N75	0.363	D31	0.557	G16	0.523
V105	0.329	H62	0.606	M103	0.364	D101	0.567	V25	0.524
N13	0.331	V111	0.611	G16	0.366	G23	0.570	N37	0.528
T8	0.332	S117	0.612	V25	0.367	K66	0.574	E65	0.528
E109	0.333	A110	0.627	H62	0.368	T18	0.576	D15	0.539
E17	0.333	N36	0.649	K66	0.371	F11	0.577	H62	0.552
E65	0.333	K66	0.671	T18	0.372	V7	0.577	E17	0.557
V9	0.333	A112	0.681	K22	0.374	H62	0.583	V107	0.566
T20	0.334	F82	0.683	D15	0.375	V111	0.584	I40	0.569
N102	0.337	A99	0.710	N86	0.377	E17	0.590	D68	0.579
D39	0.341	V114	0.729	V7	0.384	G42	0.598	K22	0.587
D27	0.342	D101	0.745	E65	0.403	T8	0.601	V7	0.588
A112	0.347	L29	0.754	A112	0.410	D15	0.610	N86	0.591
R14	0.353	G42	0.773	D101	0.416	K6	0.618	A99	0.598

D101	0.354	T97	0.799	E17	0.416	D39	0.624	T20	0.605
M103	0.355	T71	0.830	V111	0.434	A112	0.643	D39	0.606
A99	0.364	I34	0.887	R14	0.464	D61	0.651	T18	0.609
K6	0.368	I70	0.927	V114	0.476	A99	0.663	A112	0.696
D15	0.374	V25	0.963	V107	0.484	N86	0.701	K6	0.700
V107	0.398	N123	0.967	K6	0.500	V114	0.844	V114	0.958
V114	0.443			A99	0.528	N123	0.926	N123	0.964
N123	0.562			N123	0.815				
mean	0.312		0.519		0.336		0.532		0.486
SD	0.043		0.155		0.084		0.081		0.106
Mean-1SD	0.269		0.364		0.252		0.451		0.380
Mean-0.75SD	0.283		0.415		0.280		0.478		0.415

Table S2. Remaining peak intensity ratios (from free ^{15}N -rAdx) of ^{15}N -rAdx with 0.2 molar equivalents of CYP24A1 in ligand-free and ligand-bound states. Resonances are broadened more than 0.75 standard deviations (orange) or more than 1 full standard deviation (red) from the mean.

no ligand		1 to 0.4 1,25(OH) ₂ D3		1 to 0.4 1 α (OH)D3	
D79	0.241291	L57	0.366748	H62	0.340167
T85	0.260047	D68	0.377405	F59	0.427115
E74	0.265021	L80	0.382156	F82	0.433834
D76	0.269142	E73	0.387351	M103	0.441743
E73	0.27155	D79	0.396488	L80	0.460833
L84	0.273984	R89	0.405175	L57	0.473806
G83	0.274676	A81	0.405299	N75	0.477643
G42	0.27803	N75	0.408283	H10	0.48401
A81	0.27807	F59	0.408735	L29	0.484586
T71	0.282395	M77	0.409392	T85	0.485334
V32	0.28252	E74	0.411335	D72	0.504474
G26	0.282798	S28	0.416501	R89	0.508269
F82	0.284492	S117	0.416961	V107	0.508748
E35	0.285459	L19	0.417338	V33	0.511896
L29	0.285871	V32	0.418284	T21	0.520866
V33	0.286424	L38	0.418981	L78	0.52239
D31	0.28941	D76	0.42347	S117	0.523737
S88	0.289995	D31	0.427569	K12	0.529585
I70	0.290253	V33	0.427632	D76	0.53114
N37	0.291035	E35	0.43116	D27	0.537143
L78	0.29158	L84	0.432892	V32	0.53813
D61	0.294054	I70	0.433621	T97	0.539553
D72	0.294486	L67	0.44077	I34	0.549119
R87	0.295087	T85	0.440977	M77	0.549614
L80	0.29702	K12	0.450992	M100	0.554682
D41	0.297022	F43	0.451665	E65	0.557357
N75	0.298338	F11	0.454241	V9	0.558238
Y64	0.298442	V105	0.455173	L84	0.558871
L57	0.29923	I34	0.455303	E74	0.560861
N36	0.299666	L78	0.457189	G42	0.565115
S28	0.301159	N36	0.457855	A81	0.568828
L38	0.30119	V107	0.458094	R87	0.570839
V25	0.301236	N37	0.459456	N13	0.572364
M77	0.301765	D72	0.46014	N36	0.57518
K98	0.303007	S88	0.460439	G83	0.577809

K12	0.30492	D27	0.463097	D61	0.579067
L67	0.306724	T21	0.463514	G26	0.585566
I40	0.307884	H10	0.463647	T104	0.586108
F43	0.309971	V9	0.463896	T20	0.589641
A69	0.311059	I40	0.464069	E35	0.591617
T18	0.311662	D101	0.464452	L19	0.605889
F59	0.314557	T97	0.465019	D41	0.606148
G23	0.315566	F82	0.465688	A99	0.606539
D68	0.317818	T8	0.469389	L67	0.608449
K22	0.319114	E60	0.469637	V105	0.614805
T104	0.319176	M103	0.471017	F11	0.621203
G16	0.320158	G26	0.471821	T8	0.62207
E60	0.321985	Y64	0.476828	D79	0.62595
T21	0.322065	N102	0.47723	N102	0.626989
S117	0.322738	D39	0.479739	I40	0.628852
M100	0.323171	K66	0.481593	S28	0.630111
I63	0.323724	I63	0.484612	E60	0.63078
F11	0.323988	N13	0.486825	G23	0.632363
R89	0.325639	L29	0.488537	S88	0.635173
V105	0.32925	E65	0.493291	E73	0.636857
E17	0.332787	A69	0.49401	D31	0.63925
K66	0.332989	T20	0.497812	I70	0.64984
E65	0.333218	E17	0.501442	T18	0.657442
T20	0.333636	D41	0.501614	K66	0.661965
T8	0.33538	M100	0.502572	D39	0.670766
T97	0.336488	G23	0.503001	F43	0.672636
N102	0.336841	K98	0.5061	K98	0.675284
N13	0.338867	V7	0.506932	D68	0.676534
V9	0.339404	K22	0.507779	E17	0.680377
I34	0.34195	V25	0.510348	G16	0.680872
D27	0.342189	G83	0.511851	C95	0.688555
H62	0.342825	T104	0.511933	D101	0.702518
M103	0.346887	K6	0.513076	I63	0.705784
V7	0.348435	D15	0.515451	L38	0.719451
D101	0.353676	R87	0.51631	K22	0.737902
A99	0.363895	G16	0.530734	V7	0.739467
K6	0.368312	G42	0.544136	Y64	0.754254
D39	0.369648	T18	0.546604	N37	0.777652
V107	0.374371	H62	0.554238	A69	0.77845
D15	0.374481	D61	0.590073	V25	0.780875
L19	0.481258	C95	0.687759	D15	0.796437

H10	0.494986	A99	0.719571	T71	0.813488
C95	0.521859	T71	0.824187	K6	0.814359
mean	0.318349		0.474186		0.600541
SD	0.045929		0.070519		0.096721
Mean-1SD	0.272421		0.403667		0.50382
Mean-0.75SD	0.28773		0.427174		0.53606

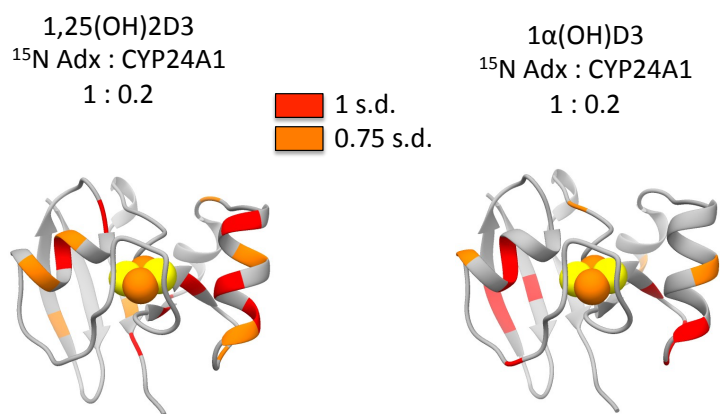


Figure S6. Mapping of the NMR peak broadening pattern observed on the HSQC spectra of ¹⁵N-Adx upon addition of 0.2 molar equivalents of ligand-bound CYP24A1.

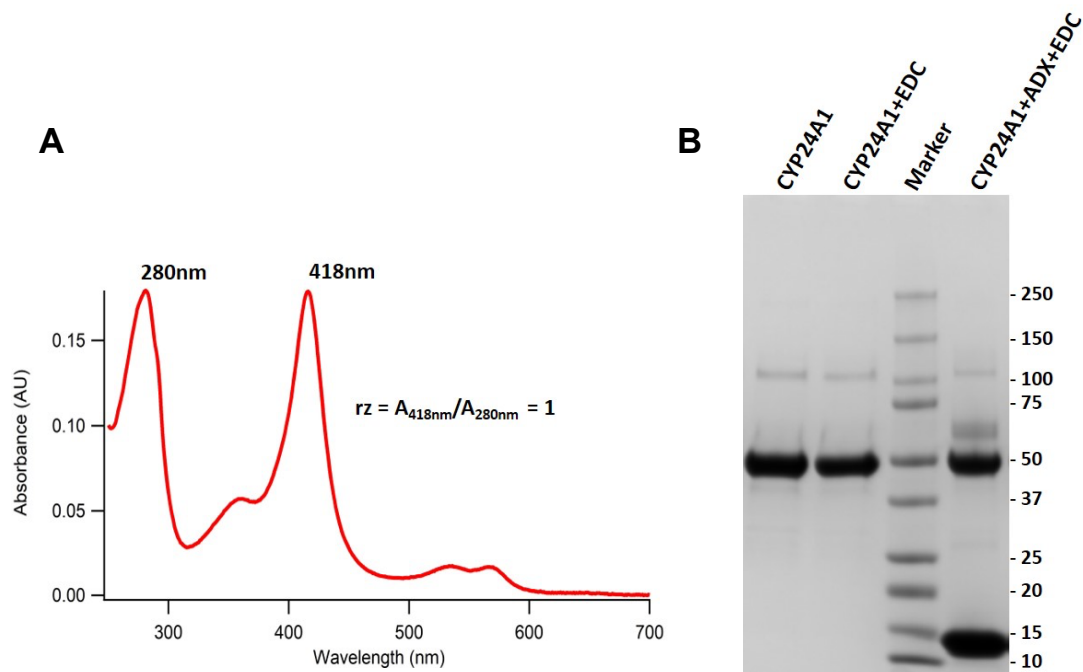


Figure S7. A) Wavelength absorption spectrum of purified CYP24A1 used in EDC cross-linking analysis. A ratio of the intensity of the Soret band to the 280 nm band indicates a high level of purity. B) SDS-PAGE of EDC-treated and untreated CYP24A1. The molecular weight values correspond to the Marker lane. The band near 100 kDa and a weak band near 30 kDa are consistent with dimerized forms of CYP24A1 and Adx, respectively, while the new band at approximately 62 kDa is consistent with the CYP24A1-Adx redox complex.

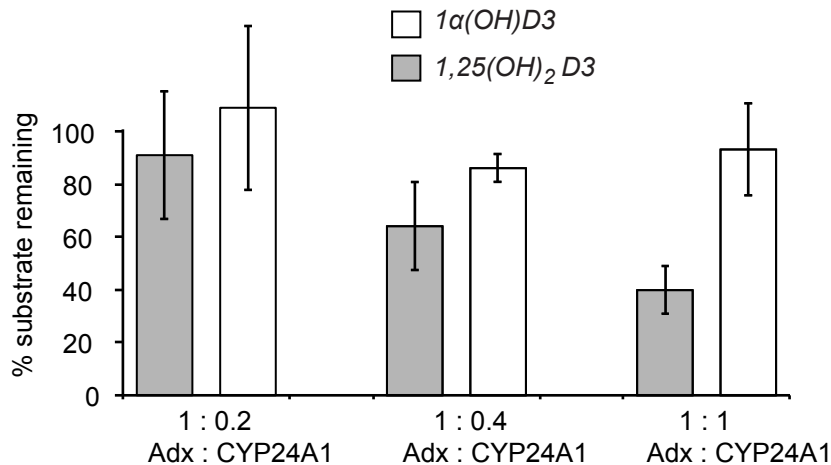


Figure S8. Effect of Adx:CYP24A1 ratio on CYP24A1-mediated catalysis of $1\alpha(\text{OH})\text{D}_3$ and $1,25(\text{OH})_2\text{D}_3$. Reconstituted assays were carried out using a constant substrate concentration ($5\ \mu\text{M}$) and with varying ratios of Adx to CYP24A1 in order to correlate with ratios of the redox partner used in NMR titrations. Due to the low turnover of substrate anticipated at low concentrations of CYP24A1 for the early titration points, the reaction time was extended from 5 minutes to 10 minutes for all ratios. As expected, increased ratios of CYP24A1 result in increased depletion of $1,25(\text{OH})_2\text{D}_3$, but not $1\alpha(\text{OH})\text{D}_3$. Notably, the non-specific protein binding observed by NMR in the presence of $1\alpha(\text{OH})\text{D}_3$ for the 1:0.4 ratio also correlates to a significant difference in the amount of substrate remaining in the functional assay.